Earthquake Geotechnical Engineering for Protection and Development of Environment and Constructions – Silvestri & Moraci (Eds)
© 2019 Associazione Geotecnica Italiana, Rome, Italy, ISBN 978-0-367-14328-2

Simulation of the slip on the fault and the trace of the 2016 Kumamoto, Japan, earthquake by dynamic fault rupturing technique

S. Dorjpalam, K. Dan & D. Ju
Ohsaki Research Institute, Inc., Japan

H. Fujiwara & N. Morikawa
National Research Institute for Earth Science and Disaster Resilience, Japan

ABSTRACT: The procedure of evaluating fault parameters for strong motion prediction published by the Headquarters for Earthquake Research Promotion, Japan, is often adopted in earthquake resistant design in Japan, and it has accumulated practical applications in Japan and other countries. However, the procedure only considers the part of a fault in the seismogenic layer and neglects the shallow part of the fault above the seismogenic layer. Most recently, Ikutama et al. (2018) showed that the shallow part of the fault must be taken into account for simulating velocity motions and permanent displacements in areas very close to a fault on the example of the 2016 Kumamoto, Japan, earthquake. In this paper we examine the slip distribution on the fault and on the fault trace of the Kumamoto earthquake by dynamic fault rupturing technique to obtain theoretical basis of the relationships among fault parameters for the shallow part of a fault.

1 INTRODUCTION

The discovery of faults in the proximity of major lifelines demands for reliable assessment tools for prediction of near-fault ground motions. The 2016 Kumamoto, Japan, earthquake provided with the opportunity to verify whether the current Recipe for strong ground motion predictions by the Headquarters for Earthquake Research Promotion (2017), Japan, can be extended to the predictions of near-field ground motions. Recent research papers on the 2016 Kumamoto earthquake (e.g., Ikutama et al. 2018) show that setting only seismogenic part of the fault, as stipulated by the Recipe, might not be enough to reproduce the near-field velocity and displacement records, and that the shallow part of the fault in the surface layers, neglected in the Recipe, actually affects greatly the near-field ground motions. The necessity of inclusion of the shallow part of a fault into the Recipe for evaluation of near-field ground motions seems undeniable, and therefore the proper fault-modeling techniques, mainly setting up slip velocity time functions, are required.

The ultimate goal of this study is to derive the shape of the slip-rate function of the shallow part of a fault based on dynamic fault rupture simulation results. As the first step towards the goal, this paper reports on the reproduction of the velocity and displacement ground motions observed at near-field distances during the Kumamoto earthquake by using dynamic fault rupturing calculations.

2 DYNAMIC FAULT MODEL FOR THE 2016 KUMAMOTO EARTHQUAKE

2.1 *Existing kinematic fault models*

Several kinematic fault models have been proposed by researchers to characterize the source of the Kumamoto earthquake. We based our dynamic fault model on the kinematic fault model

by Oana et al. (2017), which is a two-segmented fault and consists of 14 km long Hinagu segment and 28 km long Futagawa segment. The kinematic model comprises three strong motion generation areas (SMGA). The slip values for the SMGAs and the fault length were based on the source inversion results of Asano & Iwata (2016), and the stress drop values were decided by trial and error using the stochastic Green's method to reproduce the strong motion records.

2.2 *Geometry of the dynamic fault model*

For our dynamic fault model, we extended the kinematic fault model by Oana et al. (2017) along the dip up to the ground surface.

The source of the Kumamoto earthquake is a multi-segmented fault, and many researchers rightfully argue that this is the only way to set the fault model to reproduce the strong motions. However for practical reasons there is a need to explore if the approximation by a single plane fault model is viable. Therefore, we carried out dynamic simulations for three cases of the geometry of fault models. Firstly, for CASE1 we adopted two-segmented fault model as in Oana et al. (2017). Secondly, for CASE2 (Figure 1) we combined the two segments into one segment with the strike and dip angles of the more prevailing Futagawa segment. Lastly, for CASE3 we shortened CASE2 to 34 km to match the surface rupture length measured in the field by Shirahama et al. (2016).

2.3 *Dynamic fault input parameters*

We specified the shear traction within the fault area, and the main parameter defining the final slip on the fault is the dynamic stress drop.

For our dynamic simulation study, we adopted the concept of asperity model. For the asperities, we kept the sizes and the stress drop values of the SMGAs of the kinematic model and the rest of the fault area was designated as the background with the stress drop of zero (Figure 1).

When characterizing the shallow part of the fault, we tried two alternative values for the stress drop: (1) zero stress drop (CASE1, CASE2, and CASE3) and (2) negative stress drop of -5MPa (CASE1neg, CASE2neg, and CASE3neg), in order to control the slip on the fault trace.

The slip-weakening friction law was adopted as the constitutive law for our dynamic faults. As an example, Table 1 lists initial stress conditions and frictional properties on the fault for CASE2 and CASE2neg.

2.4 *Dynamic simulation conditions*

The dynamic simulations were carried out with the help of the spectral element method code SPECFEM3D developed by Komatitsch & Tromp (2002). Figure 2 illustrates an example of the simulation model CASE2, which had 15,229,620 spectral elements in total with the average grid size of 0.4 km. The minimum resolvable period was 1 second. The simulations were run on a system with eight nodes consisting of two 14-core 2.6GHz CPUs and 128GB of memory.

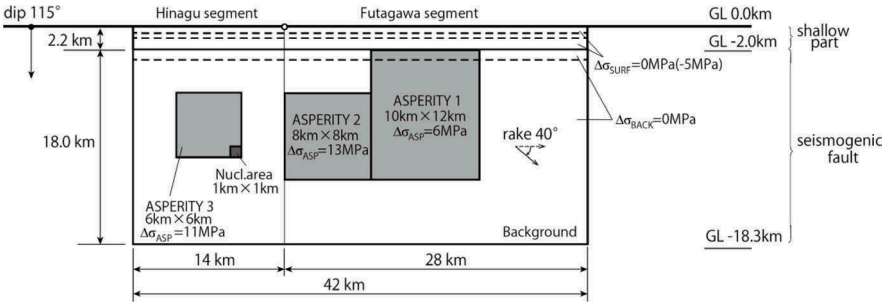

Figure 1. Dynamic fault model for the 2016 Kumamoto earthquake (CASE2 and CASE2neg).

Table 1. Dynamic fault parameters (CASE2 and CASE2neg)

		Asperity 1	Asperity 2	Asperity 3	Nucleation area	Background area	Shallow part (CASE2)	Shallow part (CASE2neg)
Initial shear stress σ_0	MPa	40.8	40.8	40.8	40.8	40.8	40.8	40.8
Initial normal stress σ_n	MPa	153.8	153.8	153.8	153.8	153.8	153.8	153.8
Strength excess SE	MPa	0.01	0.01	0.01	-0.1	0.01	0.01	0.01
Static friction coef. μ_s		0.27	0.27	0.27	0.26	0.27	0.27	0.27
Dynamic stress drop $\Delta\sigma_d$	MPa	6	13	11	11	0	0	-5
Dynamic friction coef. μ_d		0.23	0.18	0.19	0.19	0.27	0.27	0.30
Breakdown stress drop $\Delta\sigma_b$	MPa	6.01	13.01	11.01	10.9	0.01	0.01	-4.99
Critical slip D_c	cm	40	40	40	40	40	40	40

Strong ground motions were calculated at four stations shown with the red triangles in Figure 3. Two of the stations, KMMH16 (~2.2km from the fault trace) and Nishihara (~0.7km from the fault trace), recorded large peak accelerations and velocities, as well as large permanent displacements during the Kumamoto earthquake. The material on either sides of the fault was identical and linear elastic and the soil profile is given in Table 2.

3 SIMULATION RESULTS

3.1 *Slip distribution on the fault and seismic moment*

The final slip distributions for all the cases are plotted in Figure 4. Overall, the simulated final slip distributions for all the cases are similar to that of the kinematic model by Oana et al.

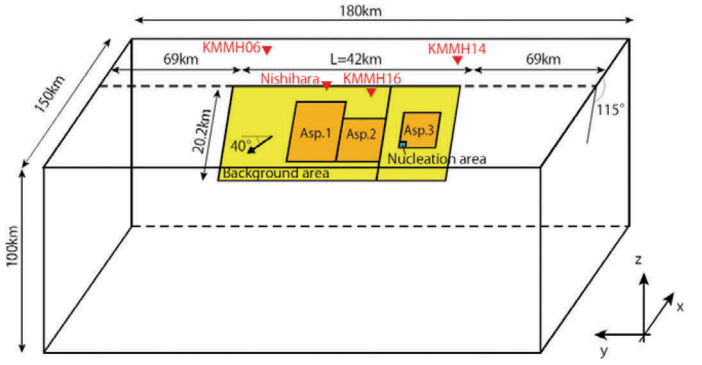

Figure 2. An example of the simulation model (CASE2 and CASE2neg).

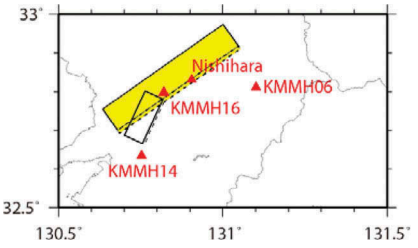

Figure 3. Location of the fault model and stations (yellow rectangle: CASE2 and CASE2neg).

Table 2. Soil profile

Layers	Depth km	S-wave velocity km/s	P-wave velocity km/s	Density t/m3
1	0.6	1.7	3.0	2.3
2	1.2	2.4	4.2	2.5
3	3.2	3.2	5.5	2.7
4	∞	3.4	6.0	2.7

(2017) and the inversion results of Asano & Iwata (2016). There are large slips on the asperities and on the ground surface immediately above them. The maximum surface slip values, which are also depicted on the slip distribution plots, for the cases with zero stress drop on the shallow part of the fault (Figure 4(a), (c), and (e) are twice the values of the cases with the negative stress drop (Figure 4(b), (d), (f)). The negative stress drop impedes the progress of the slip on the shallow part.

The seismic moments calculated from the slip distributions are summarized in Table 3. The seismic moments for the cases with zero stress drop on the shallow part are larger than the observed value published by F-net, whereas the seismic moments for the cases with the negative stress drop are closer to F-net value.

3.2 *Slip velocity time function*

The slip velocity time functions for all the three geometries of the fault models have similar trends. As an example, the slip velocity time functions on the fault for CASE2 and CASE2neg are plotted on Figure 5. There are prominent pulses on the asperities and on the shallow fault

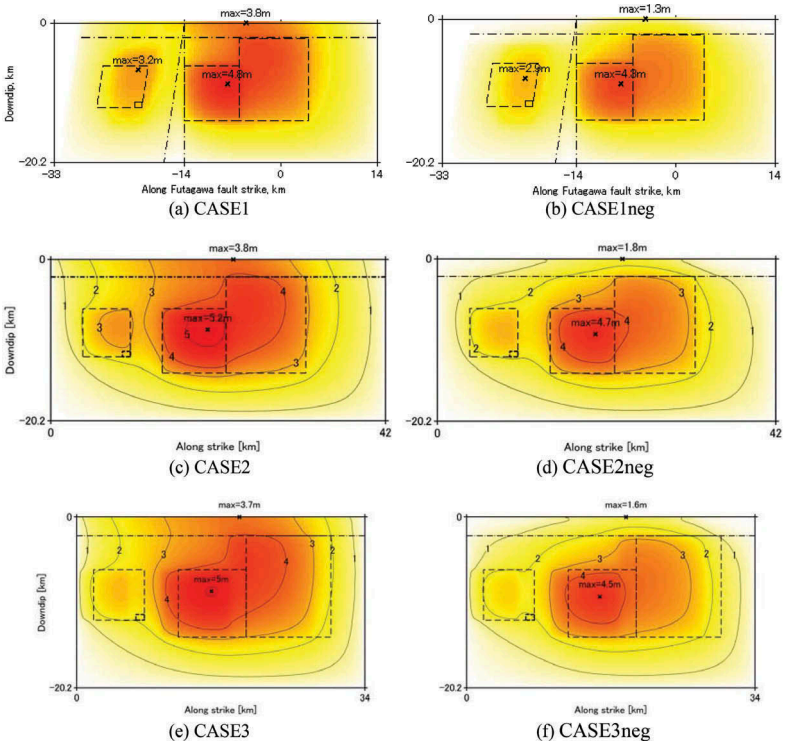

Figure 4. Final slip distribution on the fault plane

Table 3. Calculated seismic moments

Model	Simulation result N·m	Model	Simulation result N·m
CASE1	5.47E+19	CASE1neg	4.36E+19
CASE2	5.76E+19	CASE2neg	4.73E+19
CASE3	4.79E+19	CASE3neg	3.97E+19
F-net	4.42E+19		

areas above them. Especially the shallow fault area above the Asperity 1 has large pulses, which results in the excessive surface slip for CASE2, which has zero stress drops on the shallow fault part (red traces in Figure 5). On the other hand, the negative stress drop of -5MPa on the shallow part reduces the slip velocity peaks in the shallow layers by more than half (blue traces in Figure 5).

3.3 *Slip along the fault trace*

Figure 6 compares the calculated slip distributions along the fault trace with the measurements of the surface rupture conducted by Shirahama et al. (2016) after the Kumamoto earthquake. In overall, the cases with zero stress drop on the shallow part of the fault (CASE2 and CASE3) overestimate the observed surface slip, whereas the cases with the negative stress drop on the shallow part give acceptable estimations of the observed surface fault slip.

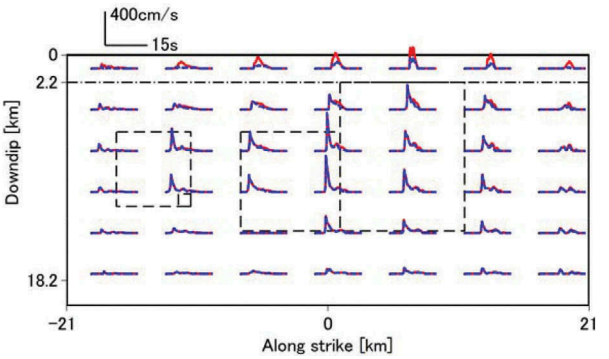

Figure 5. Simulated slip velocity time functions (red: CASE2, blue: CASE2neg).

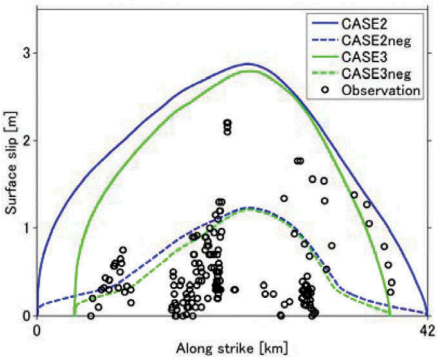

Figure 6. Comparison of the simulated horizontal fault slips along the fault trace (green and blue lines) with the observed strike-slip surface rupture (black circles).

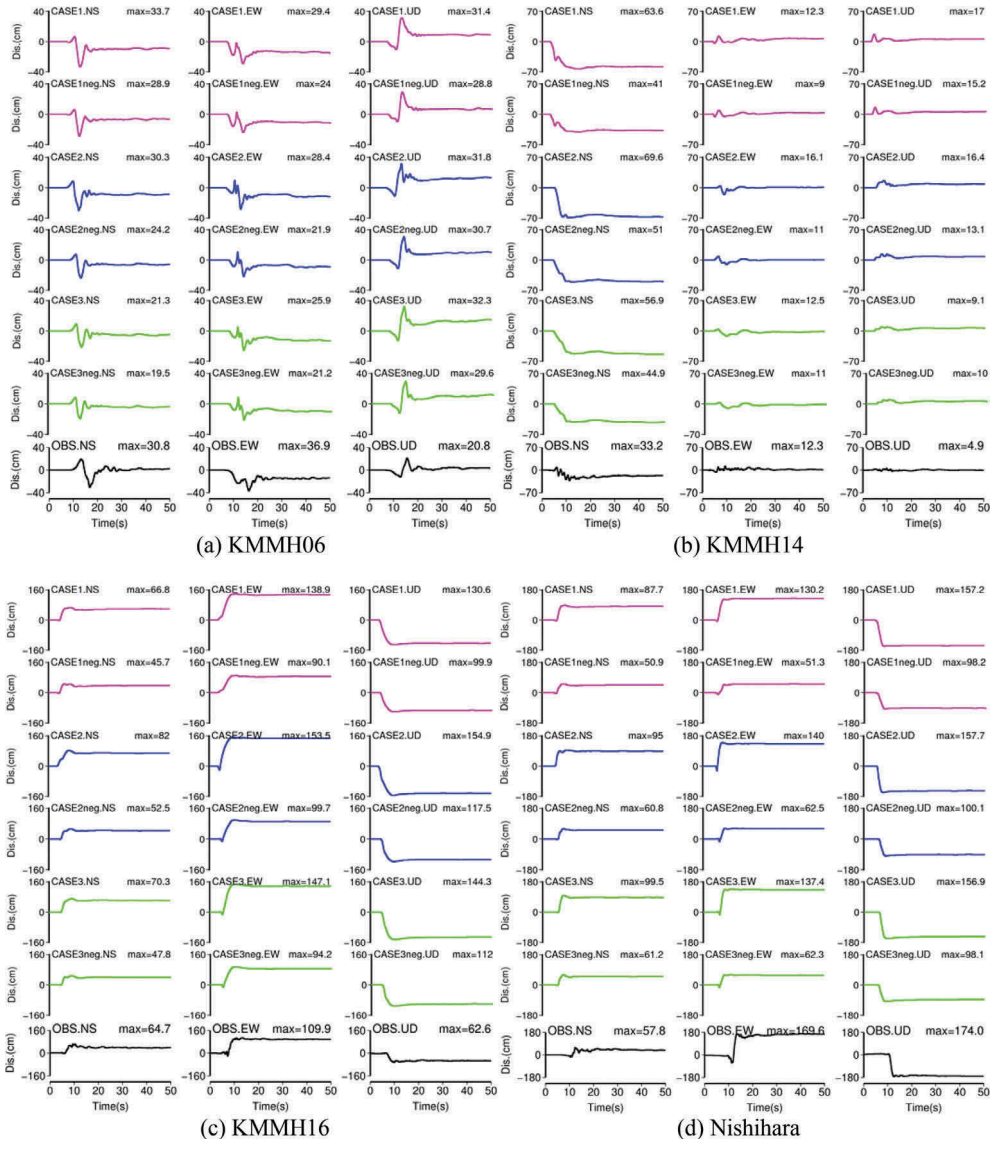

Figure 7. Comparison of the simulated and the recorded displacement waveforms (magenta: CASE1 and CASE1neg, blue: CASE2 and CASE2neg, green: CASE3 and CASE3neg, black: record).

3.4 *Simulated ground motions*

The velocity and displacement waveforms obtained from the dynamic simulations at the four stations are plotted in Figures 7 and 8, respectively. In the figures, the cases with the same geometries, but different stress drops on the shallow part, are represented with the same color lines. The cases with zero stress drop are plotted first and the cases with the negative stress drop are plotted immediately below. The observed records, against which the simulation results are compared, are plotted in black at the bottom. The velocity time series (Figure 8) were band-pass filtered in 0.05~1.0 Hz range.

Overall, for the cases with zero stress drops on the shallow part of the fault (CASE1, CASE2, and CASE3), the simulated displacement and velocity waveforms reproduce well the records in terms of the peak value and phase.

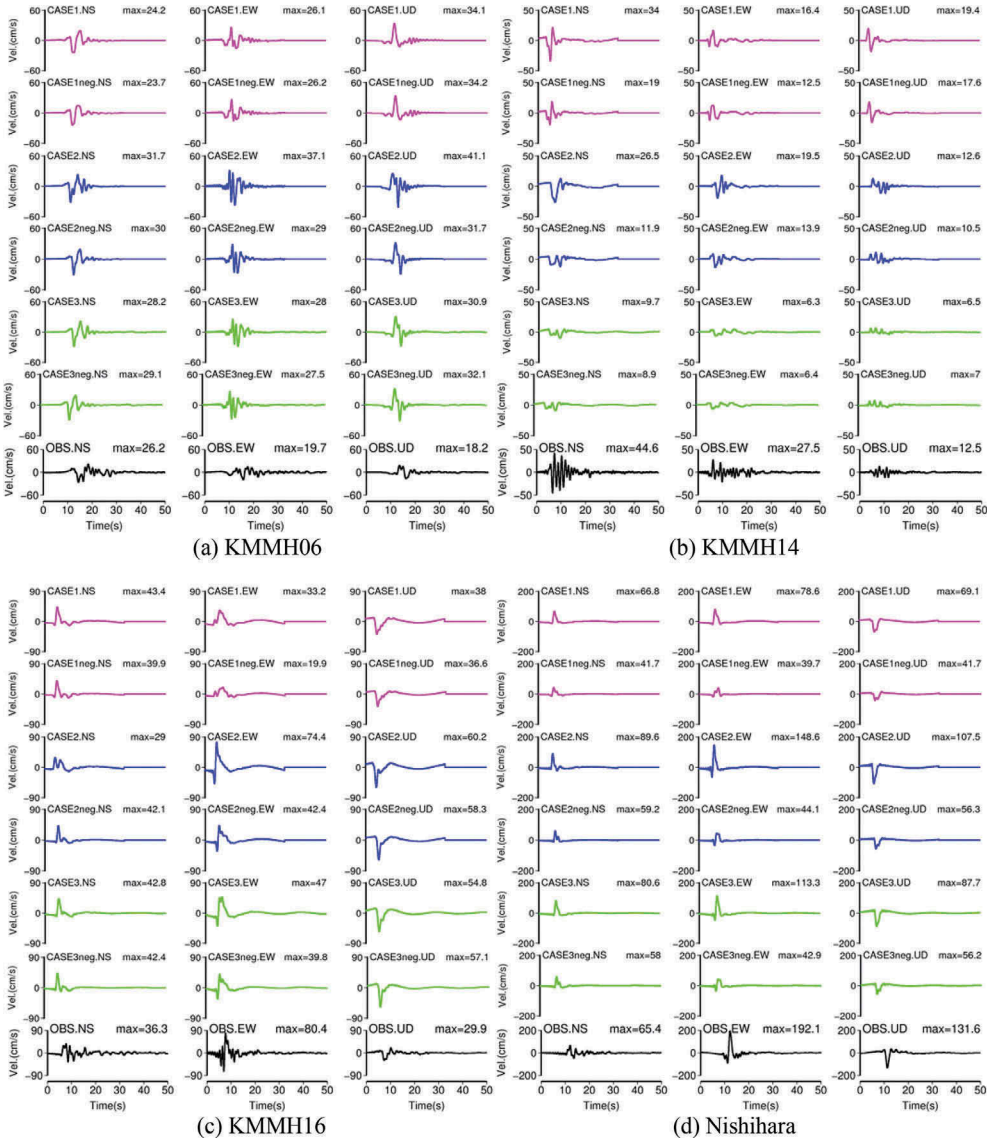

Figure 8. Comparison of the simulated and the recorded velocity waveforms (magenta: CASE1 and CASE1neg, blue: CASE2 and CASE2neg, green: CASE3 and CASE3neg, black: record).

When the negative stress drop is introduced on the shallow part of the fault (CASE1neg, CASE2neg, and CASE3neg), the peaks of the calculated waveforms are reduced by almost half at Nishihara station, which is located at 700m distance from the fault trace, and the difference lessens as the station distance from the fault trace increases.

To be able to reproduce all of the observed data, including the near-fault strong ground motions, the slip distributions along the fault trace, and the seismic moments, further tuning of the shallow part of the fault models is necessary. For example, the simple tapering of the negative stress drop of -5MPa from the surface to the top of the seismogenic layer did not lead to drastic changes in the results. On the other hand, Sakai et al. (2018) achieved very good results by impeding the slip on the fault only in the very thin (0.3 km) surface layer in their kinematic simulations.

4 CONCLUSIONS

We carried out the dynamic fault rupture simulations to reproduce the near-field ground motion and permanent displacement records of the 2016 Kumamoto earthquake. We set up three geometrically different dynamic fault models (two-segmented, one-segmented, one-segmented shortened). Because of the closeness in strike, dip, and rake angles of the two segments of the Kumamoto earthquake fault model, the simulation results, including the final slip distribution and the ground motions, did not show much sensitivity to the geometrical differences of two-segmented or one-segmented fault models.

On the other hand, the characterization of the shallow part of the faults with zero stress drop or with the negative stress drop of -5MPa directly affected the final slip on the shallow part. The zero stress drop led to the overprediction of the slip close to the ground surface, and the negative stress drop resulted in better estimation of the slip distribution. However, introduction of the negative stress drop on the shallow part of the fault models resulted in notable underprediction of the observed velocity ground motions and permanent displacements especially at Nishihara station, which is located 700m away from the fault trace. Therefore, further tuning of the dynamic characterization of the shallow part is needed to reproduce the near-fault ground motions along with other observed data, including the slip distributions along the fault trace and the seismic moment.

ACKNOWLEDGMENT

The authors gratefully acknowledge and appreciate KiK-net of National Research Institute for Earth Science and Disaster Resilience, Japan Meteorological Agency, and Kumamoto Prefecture for providing with the ground motion records.

REFERENCES

Asano, K. & Iwata, T. 2016. Source rupture processes of the foreshock and mainshock in the 2016 Kumamoto earthquake sequence estimated from the kinematic wave-form inversion of strong motion data, *Earth, Planets and Space* 68(147).

Headquarters for Earthquake Research Promotion. 2017. Strong ground motion predictions method for earthquakes with specified source faults ("Recipe"). https://www.jishin.go.jp/main/chousa/17_yosokuchizu/recipe.pdf (last accessed September 8, 2018).

Ikutama, S., Kawasato, T., Kawakami, Y., Nohsho, M., Oana, A., Dan, K., Torita, H. & Okada, Y. 2018. Source modeling for predicting ground motions and permanent displacements very close to the fault trace, *Journal of Earthquake and Tsunami* 12(5).

Komatitsch, D. & Tromp, J. 2002. Spectral-element simulations of global seismic wave propagation – I. Validation, *Geophysical Journal International* 149(2): 390–412.

Oana, A., Dan, K., Miyakoshi, J., Fujiwara, H., Morikawa, N. & Maeda, N. 2017. Estimation of characterized source model of the mainshock in the 2016 Kumamoto earthquakes using the stochastic Green's function method, 2017 Japan Geoscience Union Meeting, SCG70–P04.

Sakai, M., Ikutama, S., Sawairi, M., Oana, A., Dan, K. & Torita, H. 2018. Simulation of strong motion records considering slip of shallow fault of the 2016 Kumamoto earthquake, The 15th Japan Earthquake Engineering Symposium: OS–02–06.

Shirahama, Y., Yoshimi, M., Awata Y., Maruyama, T., Azuma, T., Miyashita, Y., Mori, H., Imanishi, K., Takeda, N., Ochi, T., Otsubo, M., Asahina, D. & Miyakawa, A. 2016. Characteristics of the surface ruptures associated with the 2016 Kumamoto earthquake sequence, central Kyushu, Japan, *Earth, Planets and Space* 68(191).